photonics

MDPI

Article

A Laser Frequency Transverse Modulation Might Compensate for the Spectral Broadening Due to Large Electron Energy Spread in Thomson Sources

Vittoria Petrillo [1,2,*], Illya Drebot [2], Geoffrey Krafft [3,4], Cesare Maroli [1], Andrea R. Rossi [2], Marcello Rossetti Conti [2], Marcel Ruijter [4,5] and Balša Terzić [4]

1 Dipartimento di Fisica, Universitá degli Studi di Milano, Via Celoria 16, 20133 Milano, Italy; Cesare.Maroli@mi.infn.it
2 INFN-Sezione di Milano, Via Celoria 16, 20133 Milano, Italy; Illya.Drebot@mi.infn.it (I.D.); Andrea.rossi@mi.infn.it (A.R.R.); Marcello.Rossetti@mi.infn.it (M.R.C.); Marcel.Ruijter@mi.infn.it (M.R.)
3 Thomas Jefferson National Accelerator Facility, Newport News, VA 23606, USA; Krafft@Jlab.com
4 Department of Physics, Center for Accelerator Science , Old Dominion University, Norfolk, VA 23529, USA; bterzic@odu.edu
5 INFN, Sezione di Roma and Dipartimento di Fisica, Universitá 'La Sapienza', Piazza Aldo Moro, 5, 00185 Roma, Italy
* Correspondence: Vittoria.Petrillo@mi.infn.it

Abstract: Compact laser plasma accelerators generate high-energy electron beams with increasing quality. When used in inverse Compton backscattering, however, the relatively large electron energy spread jeopardizes potential applications requiring small bandwidths. We present here a novel interaction scheme that allows us to compensate for the negative effects of the electron energy spread on the spectrum, by introducing a transverse spatial frequency modulation in the laser pulse. Such a laser chirp, together with a properly dispersed electron beam, can substantially reduce the broadening of the Compton bandwidth due to the electron energy spread. We show theoretical analysis and numerical simulations for hard X-ray Thomson sources based on laser plasma accelerators.

Keywords: Compton scattering; chirped laser

Citation: Petrillo, V.; Drebot, I.; Krafft, G.; Maroli, C.; Rossi, A.R.; Rossetti Conti, M.; Ruijter, M.; Terzić, B. A Laser Frequency Transverse Modulation Might Compensate for the Spectral Broadening Due to Large Electron Energy Spread in Thomson Sources. *Photonics* **2022**, *9*, 62. https://doi.org/10.3390/photonics9020062

Received: 18 December 2021
Accepted: 23 January 2022
Published: 25 January 2022

1. Introduction

X- and γ-ray radiation with significant spectral flux, high monochromaticity and wide tunability allows the deepening of the knowledge of the fundamental properties of materials and living systems by probing the matter on microscopic-to-nuclear scales in space and time. One of the processes generating X-rays is the scattering between a highly relativistic electron beam and a primary radiation source in the infrared/optical/ultraviolet range. This interaction is called Thomson scattering when the quantum recoil of the electron is negligible or inverse Compton scattering when quantum effects are important. A common use in the field is, however, to refer generically to the process with the latter name. Thomson [1–7] and inverse Compton [8,9] sources (both called ICSs) are among the most performing devices in producing X-γ radiation with high power, narrow bandwidth, large transverse coherence and tunability. Most of the existing Thomson devices, actually devoted either to experiments on the radiation characterization [10–15] or to imaging applications on biological, animal and human samples [3,16–21], generate radiation through the collision between a laser pulse and a relativistic electron beam. The maximum photon energy at the Compton edge $E_{ph,ed}$ depends on the energy of the electron beam and on the laser wavelength according to the relationship $E_{ph,ed} \approx 4\langle\gamma\rangle^2 E_{ph,L}$, $\langle\gamma\rangle$ being the mean Lorentz factor of the electron beam and $E_{ph,L}$ the energy of the laser photon.

Maximizing the photon flux and spectral density within a selected bandwidth is a primary issue in ICS operations. The relative bandwidth value $bw = \Delta E_{ph}/E_{ph}$ can be

attested at the level of a few percent in cases of imaging applications, such as mammography screening campaigns [22], but is instead required to be much smaller (down to a few 10^{-3}) in sources devoted to nuclear photonic experiments [9,23].

Extremely positive aspects of ICSs are their sustainable cost of building and maintenance and the contained global dimension of their structure. Both can be further reduced considering the option of electron beams generated by laser plasma accelerators (LPAs). These last devices have made astounding progress in generating high-energy, high-quality electron beams, [24–35] to the point that they have already been tested in the production of betatron [36–39], undulator [40–43] and SASE and seeded free-electron laser radiation [44–49]. Active research and development efforts have also been pursued to conceive compact Compton sources [50–54] based on these novel LPA accelerators. Nevertheless, due to difficulties and challenges in controlling the injection process, LPA beams, at the electron charge level of a consistent fraction of nC that is interesting for Compton sources, still present a rather large energy spread $\Delta\gamma/\langle\gamma\rangle$ of order of several percent, compromising applications requiring a high level of monochromaticity. LPA electron beams with very low energy spreads [55] seem to remain under the level of 25 pC and therefore they do not achieve the charge level necessary for Compton sources. On the other hand, a further important advantage of ICSs compared to other types of radiation sources is the large degree of freedom provided by their use in the collision of a laser pulse, instead of magnetic elements. The optical technology of pulse manipulation permits in principle to tailor the laser signal to specific needs. Various studies [56–63] have shown that the bandwidth broadening due to nonlinearities can be controlled by modulating in time the laser frequency, allowing one to push the pump intensity to large values deep inside the nonlinear regime without deteriorating the spectrum. In fact, the different laser phase values experimented by the electrons during the interaction compensate the velocity change due to the nonlinearity.

In this paper, we demonstrate how a spatial transverse frequency modulation of the laser pulse in the linear regime, combined with a proper dispersion of the electron beam, is capable of counteracting the large spectral broadening due to the energy spread. The interaction scheme investigated here is particularly suitable to LPA beams characterized by a high charge, relatively low emittance, small rms spot radius and relatively large energy spread, but can be applied to any acceleration scheme.

2. Interaction of Chirped Laser and Dispersed Electron Beam

Figure 1 presents a schematic rendering of the basic configuration of the source. In the simplest scheme, the electron beam coming from the acceleration stage (element (a) in Figure 1) is suitably dispersed in a bending magnet (b) and then refocused in a quadrupole system (c). Beam lines able to angularly disperse the electrons, while maintaining good quality, have been studied in the framework of the foreseen operations of LPA beams in FELs with transverse gradient undulators [64–67]. An example of such lines, constituted by a more sophisticated sequence of elements and that could represent an upgrade of our basic scheme, is described in detail in [68]. The laser pulse (d) is spatially chirped by inserting along its path a tilted window, or a sequence of prisms, either gratings or an equivalent device (e) able to map wavelength in position, as shown in [69], and finally focused by a telescopic system (f) to the Compton interaction point (g). The bandwidth of the emitted radiation in the linear regime, in the absence of a laser chirp and electron beam dispersion, is approximated by the expression [70]:

$$bw \approx \sqrt{\left[\frac{\Psi^2/\sqrt{12}}{1+\Psi^2/2}+\frac{2\varepsilon_n^2}{\sigma_x^2}\right]^2+\left[2\frac{\Delta\gamma}{\langle\gamma\rangle}\right]^2+\left[\frac{\Delta\omega_L}{\omega_L}\right]^2} \quad (1)$$

where the acceptance $\Psi = \gamma\theta_{acc}$ scales with the collimation angle θ_{acc}, ε_n is the emittance of the electron beam, σ_x is the rms electron dimension and $\frac{\Delta\omega_L}{\omega_L}$ the proper rms laser bandwidth.

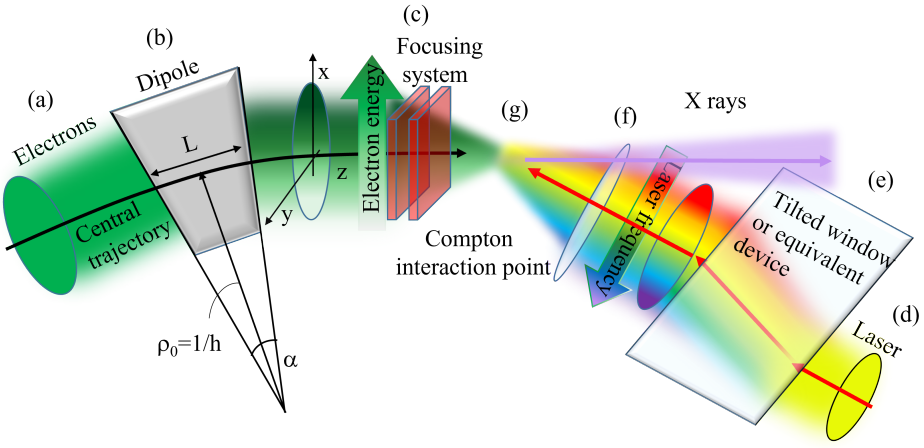

Figure 1. Dispersed electron beam and spatially chirped laser pulse in interaction: scheme and geometry of the source. (**a**) Electron beam at the exit of the acceleration stage. (**b**) Dispersive system, composed of a dipole with $\alpha = L/\rho_0$ bending angle and ρ_0 bending radius of the central orbit. (**c**) Refocusing system, composed of quadrupoles. (**d**) Laser pulse. (**e**) Spatial chirp apparatus, composed of prisms, gratings, tilted window or equivalent devices. (**f**) Laser focusing system, composed of lenses. (**g**) Compton interaction point (IP).

A large rms energy spread $\Delta\gamma/\langle\gamma\rangle$ leads to a radiation bandwidth enlargement $bw \approx 2\Delta\gamma/\langle\gamma\rangle$ that dominates the other sources of linewidth increase: acceptance, emittance and, in the usual operation without a chirp, laser polychromaticity.

While crossing a dispersive structure, the electrons acquire a transverse position distribution correlated in energy as $x - \langle x\rangle = \eta(\gamma - \langle\gamma\rangle)/\langle\gamma\rangle$ (x and γ being the coordinates and the Lorentz factor of the electrons, $\langle x\rangle$ and $\langle\gamma\rangle$ the average values).

A transverse frequency modulation of the laser $\omega_L = \omega_L(x)$ [71] can reduce the bandwidth broadening due to the energy spread.

From the resonance condition applied with the dispersed beam,

$$\omega = 4\gamma^2\omega_L \approx 4\langle\gamma\rangle^2(1 + (x - \langle x\rangle)/\eta)^2\omega_L(x), \tag{2}$$

it turns out that a transverse frequency modulation

$$\omega_L(x) = \langle\omega_L\rangle/(1 + (x - \langle x\rangle)/\eta)^2 \tag{3}$$

has the effect to compensate the inhomogeneous bandwidth broadening. This scheme, even if different in substance and applied to a different set up, recalls the transverse gradient undulator operation in free-electron lasers [72]. In the second column of Table 1, the parameters of an ideal electron beam characterized by Gaussian distributions are reported at the exit of the acceleration stage. The electron beam then crosses a dispersion section propagating within the bending magnet, acquiring an average dispersion $\eta = \sigma_x\langle\gamma\rangle/\Delta\gamma \approx 3.5 \times 10^{-5}$ and suffering from a slight increase in the emittance along x. The final characteristics of the electron beam at the Compton IP, after the refocalization provided by the final focusing system, are in the third column. In Figure 2, the beam is presented before (1), after (2) the bending and at the interaction point (3).

The electric field of the laser at $z = 0$ in the presence of the spatial frequency modulation can be written as:

$$\underline{E}_L(t, z = 0) = \underline{E}_{L0} e^{-\frac{x^2+y^2}{2\sigma_\perp^2} - \frac{c^2t^2}{2\sigma_\parallel^2}} e^{i\omega_L f(x)t} \tag{4}$$

where $\sigma_\perp$ and $\sigma_\parallel$ are, respectively, the transverse and longitudinal rms dimensions and

$$f(x) = \frac{1}{(1+\varphi(x-\langle x\rangle))^2} \tag{5}$$

is the frequency modulation along x. Regarding the laser bandwidth, it is given by two combined terms: the usual basic factor $\sigma_{L,t}$ inversely proportional to the rms laser time duration $\sigma_\parallel$ and one factor $\sigma_{L,c}$ proportional to the transverse chirp, due to the local difference in color along x. The total laser bandwidth $\Delta\omega_L$ is the quadratic combination of both.

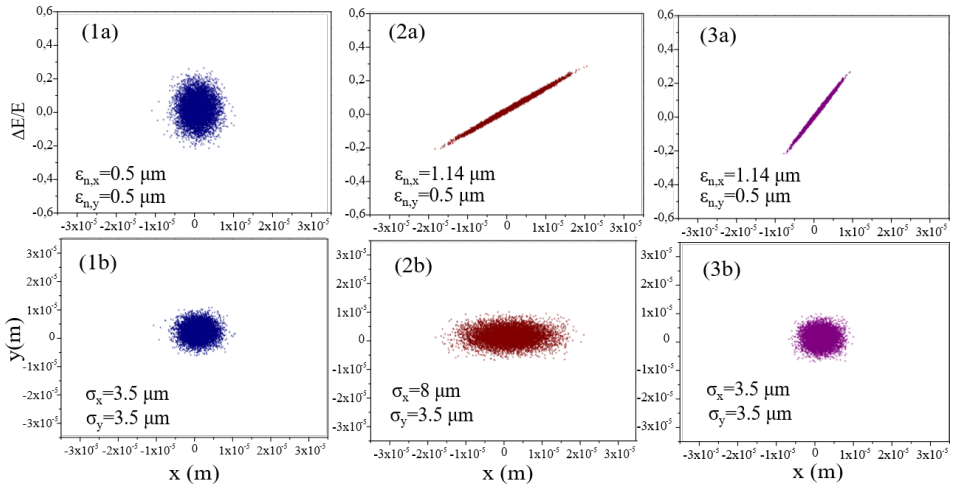

Figure 2. Electron beam: (**1a**,**1b**) after the acceleration stage; (**2a**,**2b**) after the dispersive section; (**3a**,**3b**) after the refocusing system, at the Compton interaction point. (**1a**–**3a**) Electron energy $\Delta E/E$ vs. x (m). (**1b**–**3b**) Transverse projection y (m) vs. x (m).

The shape of the laser changes during the propagation, acquiring on a long time scale a tilt and developing transverse envelope oscillations. Both these effects, which are quite small due to the short duration of the radiation process during the collision, can be minimized by containing the slope of the transverse chirp within the total laser bandwidth $\Delta\omega_L/\omega_L$«1. Regarding the time duration of the laser, we have assumed a quite long pulse of 3 ps, in order to avoid nonlinearities [73]. The laser parameter $a_0 = eE_{L0}/(mc\omega_L)$ is indeed much lower than 1, as shown in Table 1. The length of the emitted radiation, however, does not depend on the laser length. The scattered radiation by each single electron is indeed Lorentz-contracted by a factor $4\gamma^2$, and the X-pulse acquires the same short time duration of the electron beam.

Table 1. Electron, laser and radiation parameters. S is the spectral density, B the brilliance in unit u* = $s^{-1}m^{-2}rad^{-2}$/bw (0.1%).

e-Beam			**Laser**		**Radiation**	
Q (nC)	0.25	0.25	λ_L (μm)	0.8	λ_{ed} (Å)	0.013
$\langle\gamma\rangle$	391	391	$E_{ph,L}$ (eV)	1.55	$E_{ph,ed}$ (KeV)	951
$\Delta\gamma/\langle\gamma\rangle$	0.1	0.1	$\sigma_\perp$ (μm)	10	bw	0.026
σ_x (μm)	3.5	3.5	$\sigma_\parallel/c$ (ps)	3	N_{ph}	6×10^5
σ_y (μm)	3.5	3.5	a_0	0.165	S (s^{-1}/bw (0.1%))	7.6×10^{15}
$\varepsilon_{n,x}$ (μm)	0.5	1.14	E (J)	0.5	B(u*)	6.2×10^{33}
$\varepsilon_{n,y}$ (μm)	0.5	0.5	θ_{acc} (rad)	10^{-4}		

The laser parameters [6] are reported in the fifth column, and those for the scattered radiation in the seventh.

3. Numerical Results

The interaction between the electron beam and the chirped laser was investigated with the classical model based on the Liénard–Wiechert potentials. We considered the double differential energy spectrum:

$$\frac{d^2W}{d\omega d\Omega} = \frac{e^2}{4\pi^2 c}\left|\int_{-\infty}^{\infty} dt\, e^{i(!t-\underline{n}\cdot\frac{\underline{r}(t)}{c})}\left(\underline{n}\times\frac{(\underline{n}-\underline{\beta})\times\dot{\underline{\beta}}}{(1-\underline{n}\cdot\underline{\beta})^3}\right)_{ret}\right|^2 \tag{6}$$

with:

$$\dot{\underline{\beta}} = \frac{-e}{m_e c\gamma}\left[\underline{E}_L\left(1-\underline{\beta}\cdot\underline{e}_k\right)+\underline{\beta}\cdot\underline{E}_L(\underline{e}_k-\underline{\beta})\right] \tag{7}$$

where $E_L(x,y,z,t)$ is the frequency modulated electric field obtained by propagating the contour condition given by Equation (4). The interaction was assumed to be head-to-head. An angle between the electron beam and the laser pulse should have the effect of diminishing both the frequency and flux of the output radiation, and therefore it should be limited within a few degrees. The laser was transversely chirped. The total bandwidth $\Delta\omega_L$ was assumed to be about 10%, a situation that can be prepared when operating with a Ti:Sa setup.

The photon spectrum as a function of the parameter φ entering the frequency modulation of the laser with and without the chirp and dispersion apparatus is shown in Figure 3. Cases with the same total laser energy were analyzed. The acceptance angle was assumed to be $\theta_{acc} = 100\,\mu$rad. The blue curve represents the spectrum of the radiation produced by the interaction between the correlated and refocused electron beam (the one reported in Figure 2(3a,3b)) and a laser with the best chirp, corresponding to the value $\varphi = 2.9\times10^4$, close, as expected, to $1/\eta$. The black spectrum was obtained with the same electron beam, but with an unchirped laser. Intermediate cases (gray curves, with $\varphi = 1.75\times10^4$ and $\varphi = 2.2\times10^4$) are also reported for comparison. The optimum chirp case ($\varphi = 2.9\times10^4$) is in blue. The natural case, with an uncorrelated electron beam (the one reported in Figure 2(1a,1b)) and an unchirped laser pulse is in dark red. The case obtained with the same electron beam as the chirped series, but with the energy spread artificially set to zero and an unchirped laser, is represented in light red. The laser relative bandwidth, in these cases, increases from $\sigma_{L,t}/\omega_L \simeq 10^{-3}$ for the no chirp case to $\Delta\omega_L/\omega_L \simeq 10\%$. In the absence of a chirp, with 10^{-3} of laser bandwidth, without correlation between energy and the x-coordinate, the radiation bandwidth approaches 25%. The presence of the transverse frequency modulation allows an optimum recovery of the spectral shape, which arrives with a bandwidth bw = 2.67%, quite close to the value obtained with the beam with the same shape and emittance but with the energy spread artificially set to zero and the laser without a chirp and a factor 10 narrower than without a chirp. The bandwidth values (red triangles) and the photon numbers (black squares) are presented in Figure 4 as a function of the frequency modulation parameter φ. On the left side, the triangles and the squares represent the bandwidths and the photon numbers of the natural case, with the laser without a chirp and the electron beam without dispersion shown in Figure 2a, and of the artificial case, obtained by suppressing the energy spread of the aforementioned beam. In both these reference situations, the photon number is larger than in the cases with chirped laser and dispersed electrons. The number of photons is indeed inversely proportional to the sum of the laser and electron areas during the scattering and the case with electron dispersion and chirped laser is characterized by a larger beam intersection area in the interaction point. Moreover, the correlation between energy and the x-coordinateproduces an asymmetry of the radiation pattern in the azimuthal angle, which entails a slightly narrower bandwidth also in the absence of a chirp. However, other broadening factors, such as the electron emittance and the intrinsic angle energy correlation term, limit the values of the bandwidth that can be achieved. Effects like jitters or the pointing instability increase the bandwidth

as well and decrease the flux. Cases with a lower energy spread can still take advantage from this method. Using the same beam, but with an energy spread at 2.5%, collecting the radiation in an acceptance angle of 0.6 mrad leads to a bandwidth of about 7.5%. Electron dispersion and laser transverse chirp decrease it to 4%, the incomplete compensation of the energy spread factor being due to the increase of the emittance term. This method is suitable for imaging application. It should not, however, be able to generate gamma radiation with a 10^{-3} relative bandwidth such as for nuclear photonics, a regime that, when reached, needs the strict optimization of a linac high-charge electron beam to energy spread of few 10^{-4}, emittances below 0.5 μm and the use of a narrow bandwidth laser [8,9].

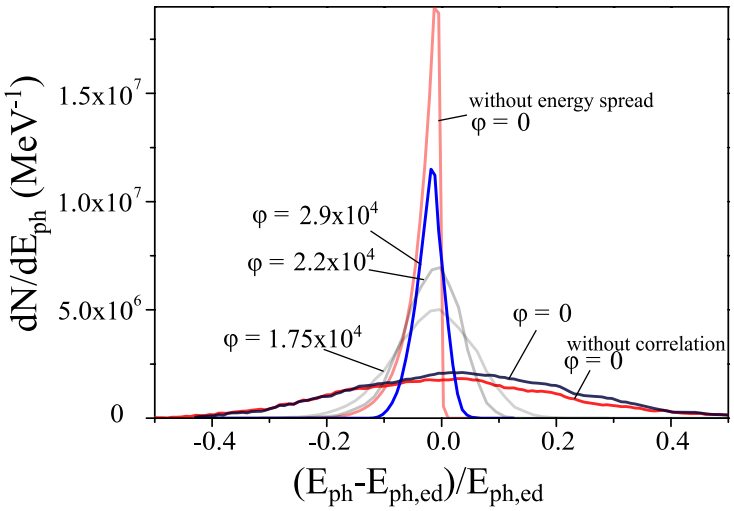

Figure 3. Number of photon density dN/dE_{ph} vs. $(E_{ph} - E_{ph,ed})/E_{ph,ed}$ as a function of the modulation coefficient φ, for acceptance angle $\theta_{acc} = 100\,\mu$rad. The natural case with no correlation between energy and x-coordinate and no chirp (red curve) is compared with the correlated electron beam with no chirped laser (black curve) and with increasingly chirped laser (gray curves with, respectively, $\varphi = 1.75 \times 10^4$ and $\varphi = 2.2 \times 10^4$). In light red, the interaction between a not chirped laser with the same electron beam as the chirped cases, but with energy spread artificially set to zero.

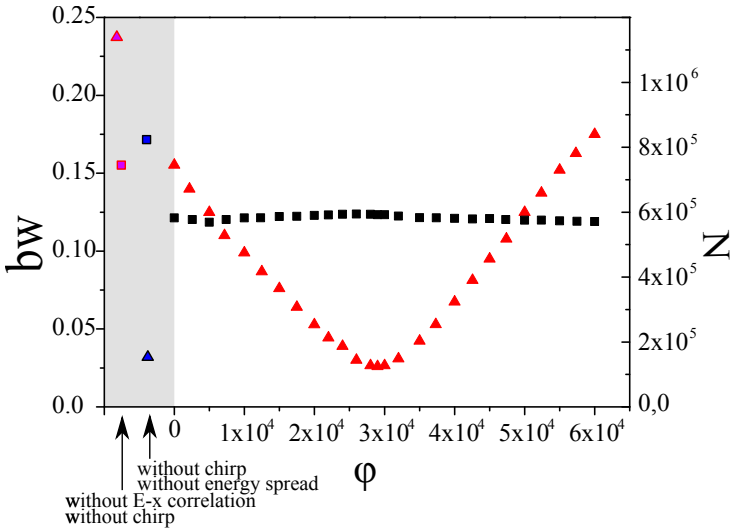

Figure 4. Bandwidth bw (triangles on the left axis) and photon number N (squares on the right axis) as a function of the parameter φ appearing in the frequency modulation. The acceptance angle is $\theta_{acc} = 100\,\mu$rad. In the gray sector, the cases without correlation between energy and x-coordinate and chirp, with and without energy spread are shown.

4. Conclusions

In conclusion, we demonstrate that a spatial transverse frequency modulation, combined with suitable dispersion-refocusing stages of the electron beam, is able to compensate the bandwidth broadening associated with the electron energy spread, decreasing the bandwidth by a factor of order 10, maintaining the same photon yield, with a consequent increase in the spectral density. This technique is particularly suitable in the operation of Compton scattering sources based on plasma acceleration electron beams.

Author Contributions: Conceptualization, V.P., C.M., G.K. and B.T.; methodology, I.D., M.R., M.R.C.; writing—original draft preparation, V.P. Investigation, V.P., I.D., G.K., C.M., A.R.R., M.R.C., M.R. and B.T. All authors have read and agreed to the published version of the manuscript.

Funding: This research received no external funding.

Conflicts of Interest: The authors declare no conflict of interest.

References

1. Pogorelsky, I.V.; Ben-Zvi, I.; Hirose, T.; Kashiwagi, S.; Yakimenko, V.; Kusche, K.; Siddons, P.; Skaritka, J.; Kumita, T.; Tsunemi, A.; et al. Demonstration of 8 × 10 18 photons/second peaked at 1.8 A in a relativistic Thomson scattering experiment. *PPhys. Rev. Spec. Top.-Accel. Beams* **2000**, *3*, 090702. [CrossRef]
2. Brown, W.J.; Anderson, S.G.; Barty, C.P.J.; Betts, S.M.; Booth, R.; Crane, J.K.; Cross, R.R.; Fittinghoff, D.N.; Gibson, D.J.; Hartemann, F.V.; et al. Experimental characterization of an ultrafast Thomson scattering x-ray source with three-dimensional time and frequency-domain analysis. *Phys. Rev. Spec. Top.-Accel. Beams* **2004**, *7*, 060702. [CrossRef]
3. Bech, M.; Bunk, O.; David, C.; Ruth, R.; Rifkin, J.; Loewen, R.; Feidenhans'l, R.; Pfeiffer, F. Hard X-ray phase-contrast imaging with the Compact Light Source based on inverse Compton X-rays. *J. Synchrotron Rad.* **2009**, *16*, 43. [CrossRef]
4. Kuroda, R.; Toyokawa, H.; Yasumoto, M.; Ikeura-Sekiguchi, H.; Koike, M.; Yamada, K.; Yanagida, T.; Nakajyo, T.; Sakai, F.; Mori, K. Quasi-monochromatic hard X-ray source via laser Compton scattering and its application. *Nucl. Instrum. Methods Phys. Res.* **2011**, *A637*, S183–S186. [CrossRef]
5. Du, Y.; Yan, L.; Hua, J.; Du, Q.; Zhang, Z.; Li, R.; Qian, H.; Huang, W.; Chen, H.; Tang, C. Generation of first hard X-ray pulse at Tsinghua Thomson Scattering X-ray Source. *Rev. Sci. Instrum.* **2013**, *84*, 053301. [CrossRef]
6. Vaccarezza, C.; Alesini, D.; Anania, M.P.; Bacci, A.; Biagioni, A.; Bisesto, F.; Bellaveglia, M.; Cardarelli, P.; Cardelli, F.; Cianchi, A. The SPARC_LAB Thomson source. *Nucl. Instr. Meth. Phys. Res. A* **2016**, *829*, 237–242. [CrossRef]
7. Eggl, E.; Dierolf, M.; Achterhold, K.; Jud, C.; Guether, B.; Braig, E.; Gleich, B.; Pfeiffer, F. The Munich Compact Light Source: Initial performance measures. *J. Synchrotron Radiat.* **2016**, *23*, 1137–1142. [CrossRef]
8. Sun, C.; Wu, Y.K. Theoretical and simulation studies of characteristics of a Compton light source. *Phys. Rev. Spec. Top.-Accel. Beams* **2011**, *14*, 044701. [CrossRef]
9. EuroGammaS. Technical Design Report for the ELI_np Gamma beam System. *arXiv* **2014**, arXiv:1407.3669.
10. Babzien, M.; Ben-Zvi, I.; Kusche, K.; Pavlishin, I.V.; Pogorelsky, I.V.; Siddons, D.P.; Yakimenko, V.; Cline, D.; Zhou, F.; Hirose, T.; et al. Observation of the Second Harmonic in Thomson Scattering from Relativistic Electrons. *Phys. Rev. Lett.* **2006**, *96*, 054802. [CrossRef]
11. Ikeura-Sekiguchi, H.; Kuroda, R.; Yasumoto, M.; Toyokawa, H.; Koike, M.; Yamada, K.; Sakai, F.; Mori, K.; Maruyama, K.; Oka, H.; et al. In-line phase-contrast imaging of a biological specimen using a compact laser-Compton scattering-based x-ray source. *Appl. Phys. Lett.* **2008**, *92*, 131107. [CrossRef]
12. Sakai, Y.; Pogorelsky, I.; Williams, O.; O'Shea, F.; Barber, S.; Gadjev, I.; Duris, J.; Musumeci, P.; Fedurin, M.; Korostyshevsky, A.; et al. Observation of redshifting and harmonic radiation in inverse Compton scattering. *Phys. Rev. Spec. Top.-Accel. Beams* **2015**, *18*, 060702. [CrossRef]
13. Sakai, Y.; Gadjev, I.; Hoang, P.; Majernik, N.; Nause, A.; Fukasawa, A.; Williams, O.; Fedurin, M.; Malone, B.; Swinson, C.; et al. Single shot, double differential spectral measurements of inverse Compton scattering in the nonlinear regime *Phys. Rev. Accel. Beams* **2017**, *20*, 060701. [CrossRef]
14. Krämer, J.M.; Jochmann, A.; Budde, M.; Bussmann, M.; Couperus, J.P.; Cowan, T.E.; Debus, A.; Köhler, A.; Kuntzsch, M.; García, A.L.; et al. Making spectral shape measurements in inverse Compton scattering a tool for advanced diagnostic applications. *Sci. Rep.* **2018**, *8*, 1398. [CrossRef]
15. Yan, W.; Fruhling, C.; Golovin, G.; Haden, D.; Luo, J.; Zhang, P.; Zhao, B.; Zhang, J.; Liu, C.; Chen, M.; et al. High-order multiphoton Thomson scattering. *Nat. Photonics* **2017**, *11*, 514–520. [CrossRef]
16. Achterhold, K.; Bech, M.; Schleede, S.; Potdevin, G.; Ruth, R.; Loewen, R.; Pfeiffer, F. Monochromatic computed tomography with a compact laser-driven X-ray source. *Sci. Rep.* **2013**, *3*, 1313. [CrossRef]
17. Golosio, B.; Endrizzi, M.; Oliva, P.; Delogu, P.; Carpinelli, M.; Pogorelsky, I.; Yakimenko, V. Measurement of an inverse Compton scattering source local spectrum using k-edge filters. *Appl. Phys. Lett.* **2012**, *100*, 164104. [CrossRef]

18. Meinel, F.G.; Schwab, F.; Schleede, S.; Bech, M.; Herzen, J.; Achterhold, K.; Auweter, S.; Bamberg, F.; Yildirim, A.O.; Bohla, A.; et al. Diagnosing and mapping pulmonary emphysema on X-ray projection images: incremental value of grating-based X-ray dark-field imaging. *PLoS ONE* **2013**, *8*, 59526.
19. Schwab, F.; Schleede, S.; Hahn, D.; Bech, M.; Herzen, J.; Auweter, S.; Bamberg, F.; Achterhold, K.; Yildirim, A.O.; Bohla, A.; et al. Comparison of contrast-to-noise ratios of transmission and dark-field signal in grating-based X-ray imaging for healthy murine lung tissue. *Z. Fuer Mediznische Phys.* **2013**, *23*, 236–242. [CrossRef]
20. Vagberg, W.; Larsson, D.H.; Li, M.; Arner, A.; Hertz, H.M. X-ray phase-contrast tomography for high-spatial-resolution zebrafish muscle imaging. *Sci. Rep.* **2015**, *5*, 16625. [CrossRef]
21. Eggl, E.; Mechlem, K.; Braig, E.; Kulpe, S.; Dierolf, M.; Gunther, B.; Achterhold, K.; Herzen, J.; Gleich, B.; Rummeny, E.; et al. Mono-energy coronary angiography with a compact synchrotron source. *Sci. Rep.* **2017**, *7*, 42211. [CrossRef] [PubMed]
22. Oliva, P.; Bacci, A.; Bottigli, U.; Carpinelli, M.; Delogu, P.; Ferrario, M.; Giulietti, D.; Golosio, B.; Petrillo, V.; Serafini, L.; et al. Start-to-end simulation of a Thomson source for mammography. *Nucl. Instrum. Methods Phys. Res. Sect. A Accel. Spectrometers Detect. Assoc. Equip.* **2010**, *615*, 93–99. [CrossRef]
23. Petrillo, V.; Bacci, A.; Curatolo, C.; Drebot, I.; Giribono, A.; Maroli, C.; Rossi, A.R.; Serafini, L.; Tomassini, P.; Vaccarezza, C.; et al. Polarization of x-gamma radiation produced by a Thomson and Compton inverse scattering. *Phys. Rev. Spec. Top.-Accel. Beams* **2015**, *18*, 110701. [CrossRef]
24. Faure, J.; Rechatin, C.; Norlin, A.; Lifschitz, A.; Glinec, Y.; Malka, V. Controlled injection and acceleration of electrons in plasma wakefields by colliding laser pulses. *Nature* **2006**, *444* , 737–739. [CrossRef]
25. Lu, W.; Tzoufras, M.; Joshi, C.; Tsung, F.; Mori, W.; Vieira, J.; Fonseca, J.R.; Silva, L. Generating multi-GeV electron bunches using single stage laser wakefield acceleration in a 3D nonlinear regime. *Phys. Rev. Spec. Top.-Accel. Beams* **2007**, *10* , 061301. [CrossRef]
26. Lundh, O.; Lim, J.; Rechatin, C.; Ammoura, L.; Ben-Ismail, A.; Davoine, X.; Gallot, G.; Goddet, J.; Lefebvre, E.; Malka, V.; et al. Few femtosecond, few kiloampere electron bunch produced by a laser-plasma accelerator. *Nat. Phys.* **2011**, *7*, 219–222. [CrossRef]
27. Faure, J.; Rechatin, C.; Lundh, O.; Ammoura, L.; Malka, V. Injection and acceleration of quasi monoenergetic relativistic electron beams using density gradients at the edges of a plasma channel. *Phys. Plasmas* **2011**, *8*, 083107.
28. Corde, S.; Thaury, C.; Lifschitz, A.; Lambert, G.; Phuoc, K.T.; Davoine, X.; Lehe, R.; Douillet, D.; Rousse, A.; Malka, V. Observation of longitudinal and transverse self-injections in laser-plasma accelerators. *Nat. Commun.* **2013**, *4*, 1501. [CrossRef]
29. Thaury, C.; Guillaume, E.; Lifschitz, A.; Phuoc, K.T.; Hansson, M.; Grittani, G.; Gautier, J.; Goddet, J.-P.; Tafzi, A.; Lundh, O.; et al. Shock assisted ionization injection in laser-plasma accelerators. *Sci. Rep.* **2015**, *5*, 16310. [CrossRef]
30. Geddes, C.G.R.; Nakamura, K.; Plateau, G.R.; Toth, C.; Cormier-Michel, E.; Esarey, E.; Schroeder, C.B.; Cary, J.R.; Leemans, W.P. Plasma-density-gradient injection of low absolute-momentum-spread electron bunches. *Phys. Rev. Lett.* **2008**, *100*, 215004. [CrossRef]
31. Leemans, W.P.; Gonsalves, A.J.; Mao, H.-S.; Nakamura, K.; Benedetti, C.; Schroeder, C.B.; Toeth, C.; Daniels, J.; Mittelberger, D.E.; Bulanov, S.S.; et al. Multi-GeV electron beams from capillary-discharge-guided subpetawatt laser pulses in the self-trapping regime. *Phys. Rev. Lett.* **2014**, *113*, 245002. [CrossRef] [PubMed]
32. Kalmykov, S.; Yi, S.A.; Khudik, V.; Shvets, G. Electron self-injection and trapping into an evolving plasma bubble. *Phys. Rev. Lett.* **2009**, *103*, 135004. [CrossRef] [PubMed]
33. Pollock, B.B.; Clayton, C.E.; Ralph, J.E.; Albert, F.; Davidson, A.; Divol, L.; Filip, C.; Glenzer, S.H.; Herpoldt, K.; Lu, W.; et al. Demonstration of a narrow energy spread, electron beam from a two-stage laser wakefield accelerator. *Phys. Rev. Lett.* **2011**, *107*, 045001. [CrossRef] [PubMed]
34. Weingartner, R.; Raith, S.; Popp, A.; Chou, S.; Wenz, J.; Khrennikov, K.; Heigoldt, M.; Maier, A.; Kajumba, N.; Fuchs, M.; et al. Ultralow emittance electron beams from a laser-wakefield accelerator. *Phys. Rev. Spec. Top.-Accel. Beams* **2012**, *15*, 111302. [CrossRef]
35. Andre, T.; Andriyash, I.A.; Loulergue, A.; Labat, M.; Roussel, E.; Ghaith, A.; Khojoyan, M.; Thaury, C.; Valleau, M.; Briquez, F. et al. Control of laser plasma accelerated electrons for light sources. *Nat. Comm.* **2018**, *9*, 1334. [CrossRef]
36. Cipiccia, S.; Islam, M.R.; Ersfeld, B.; Shanks, R.P.; Brunetti, E.; Vieux, G.; Yang, X.; Issac, R.C.; Wiggins, S.M.; Welsh, G.H.; et al. Gamma-rays from harmonically resonant betatron oscillations in a plasma wake. *Nat. Phys.* **2011**, *7*, 867–871. [CrossRef]
37. Kneip, S.; McGuffey, C.; Martins, J.L.; Martins, S.F.; Bellei, C.; Chvykov, V.; Dollar, F.; Fonseca, R.; Huntington, C.; Kalintchenko, G.; et al. Bright spatially coherent synchrotron X-rays from a table-top source. *Nat. Phys.* **2010**, *6*, 980–983. [CrossRef]
38. Corde, S.; Phuoc, K.T.; Lambert, G.; Fitour, R.; Malka, V.; Rousse, A.; Beck, A.; Lefebvre, E. Femtosecond x rays from laser-plasma accelerators. *Rev. Mod. Phys.* **2013**, *85*, 1. [CrossRef]
39. Albert, F.; Thomas, A.G.R. Applications of laser wakefield accelerator-based light sources. *Plasma Phys. Control Fusion* **2016**, *58*, 103001. [CrossRef]
40. Schlenvoigt, H.-P.; Haupt, K.; Debus, A.; Budde, F.; Jaekel, O.; Pfotenhauer, S.; Schwoerer, H.; Rohwer, E.; Gallacher, J.; Brunetti, E.; et al. A compact synchrotron radiation source driven by a laser-plasma wakefield accelerator. *Nat. Phys.* **2008**, *4*, 130–133. [CrossRef]
41. Fuchs, M.; Weingartner, R.; Popp, A.; Major, Z.; Becker, S.; Osterhoff, J.; Cortrie, I.; Zeitler, B.; Hoerlein, R.; Tsakiris, G.D.; et al. Laser-driven soft-X-ray undulator source. *Nat. Phys.* **2009**, *5*, 826–829. [CrossRef]

42. Lambert, G.; Corde, S.; Phuoc, K.T.; Malka, V.; Ismail, A.B.; Benveniste, E.; Specka, A.; Labat, M.; Loulergue, A.; Bachelard, R.; et al. Progress on the generation of undulator radiation in the UV from a plasma-based electron beam. In Proceedings of the FEL2012, Nara, Japan, 26–31 August 2012; p. 2.
43. LUX. Available online: http://lux.cfel.de/index.htm (accessed on 20 November 2021).
44. Walker, P.A.; Alesini, P.D.; Alexandrova, A.S.; Anania, M.P.; Andreev, N.E.; Andriyash, I.; Aschikhin, A.; Assmann, R.W.; Audet, T.; Bacci, A.; et al. Horizon 2020 EuPRAXIA design study. *J. Phys. Conf. Ser.* **2017**, *874*, 012029 [CrossRef]
45. Ferrario, M.; Alesini, D.; Anania, M.P.; Artioli, M.; Bacci, A.; Bartocci, S.; Bedogni, R.; Bellaveglia, M.; Biagioni, A.; Bisesto, F.; et al. EuPRAXIA@ SPARC_LAB Design study towards a compact FEL facility at LNF. *Nucl. Instrum. Methods Phys. Res. Sect. A Accel.* **2018**, *909*, 134–138. [CrossRef]
46. Wang, W.; Feng, K.; Ke, L.; Yu, C.; Xu, Y.; Qi, R.; Chen, Y.; Qin, Z.; Zhang, Z.; Fang, M.; et al. Free-electron lasing at 27 nanometres based on a laser wakefield accelerator. *Nature* **2021**, *595*, 516–520. [CrossRef]
47. Pompili, R. First lasing of a free-electron laser with a compact beam-driven plasma accelerator. *Nat. Phys.* **2021**, *submitted*.
48. Galletti, M. Stable Operation of a Free-Electron Laser Driven by a Plasma Accelerator. *in preparation*.
49. Powers, N.D.; Ghebregziabher, I.; Golovin, G.; Liu, C.; Chen, S.; Banerjee, S.; Zhang, J.; Umstadter, D.P. Quasi-monoenergetic and tunable X-rays from a laser-driven Compton light source. *Nat. Photonics* **2014**, *8*, 28–31. [CrossRef]
50. Chen, S.; Powers, N.D.; Ghebregziabher, I.; Maharajan, C.; Liu, C.; Golovin, G.; Banerjee, S.; Zhang, J.; Cunningham, N.; Moorti, A.; et al. MeV-Energy X Rays from Inverse Compton Scattering with Laser-Wakefield Accelerated Electrons. *Phys. Rev. Lett.* **2013**, *110*, 155003. [CrossRef]
51. Sarri, G.; Corvan, D.J.; Schumaker, W.; Cole, J.M.; Piazza, A.D.; Ahmed, H.; Harvey, C.; Keitel, C.H.; Krushelnick, K.; Mangles, S.D.; et al. Ultrahigh Brilliance Multi-MeV g-rays Beams from Nonlinear Relativistic Thomson Scattering. *Phys.Rev. Lett.* **2014**, *113*, 224801. [CrossRef]
52. Schwoerer, H.; Liesfeld, B.; Schlenvoigt, H.-P.; Amthor, K.-U.; Sauerbrey, R. Thomson-Backscattered X Rays From Laser-Accelerated Electrons. *Phys. Rev. Lett.* **2006**, *96*, 014802. [CrossRef]
53. Khrennikov, K.; Wenz, J.; Buck, A.; Xu, J.; Heigoldt, M.; Veisz, L.; Karsch, S. Tunable All-Optical Quasimonochromatic Thomson X-Ray Source in the Nonlinear Regime. *Phys. Rev. Lett.* **2015**, *114*, 195003. [CrossRef]
54. Phuoc, K.T.; Corde, S.; Thaury, C.; Malka, V.; Tafzi, A.; Goddet, J.P.; Shah, R.C.; Sebban, S.; Rousse, A. All-optical Compton gamma-ray source. *Nat. Photonics* **2012**, *6*, 308–311. [CrossRef]
55. Ke, L.T.; Feng, K.; Wang, W.T.; Qin, Z.Y.; Yu, C.H.; Wu, Y.; Chen, Y.; Qi, R.; Zhang, Z.J.; Xu, Y.; et al. Near-GeV Electron Beams at a Few Per-Mille Level from a Laser Wakefield Accelerator via Density-Tailored Plasma. *Phys. Rev. Lett.* **2021**, *126*, 214801. [CrossRef]
56. Ghebregziabher, I.; Shadwick, B.A.; Umstadter, D. Spectral bandwidth reduction of Thomson scattered light by pulse chirping. *Phys. Rev. Spec. Top.-Accel. Beams* **2013**, *16*, 030705. [CrossRef]
57. Terzić, B.; Deitrick, K.; Hofler, A.; Krafft, G.A. Narrow-band emission in Thomson sources operating in the high-field regime. *Phys. Rev. Lett.* **2014**, *112*, 074801. [CrossRef]
58. Terzić, B.; Reeves, C.; Krafft, G.A. Combining harmonic generation and laser chirping to achieve high spectral density in Compton sources. *Phys. Rev. Spec. Top.-Accel. Beams* **2016**, *19*, 044403. [CrossRef]
59. Rykovanov, S.G.; Geddes, C.G.R.; Schroeder, C.B.; Esarey, E.; Leemans, W.P. Controlling the spectral shape of nonlinear Thomson scattering with proper laser chirping. *Phys. Rev. Spec. Top.-Accel. Beams* **2016**, *19*, 030701. [CrossRef]
60. Maroli, C.; Petrillo, V.; Drebot, I.; Serafini, L.; Terzić, B.; Krafft, G.A. Compensation of non-linear bandwidth broadening by laser chirping in Thomson sources. *J. Appl. Phys.* **2018**, *124*, 063105. [CrossRef]
61. Terzić, B.; Krafft, G.; Brown, A.; Drebot, I.; Hagerman, T.; Johnson, E.; Krafft, G.A.; Maroli, C.; Petrillo, V.; Ruijter, M. Improving performance of inverse Compton sources through laser chirping. *Europhys. Lett.* **2019**, *126*, 12003. [CrossRef]
62. Seipt, D.; Kharin, V.Y.; Rykovanov, S.G. Optimizing Laser Pulses for Narrow-Band Inverse Compton Sources in the High-Intensity Regime. *Phys. Rev. Lett.* **2019**, *122*, 204802. [CrossRef]
63. Ruijter, M.; Petrillo, V.; Zepf, M. Decreasing the bandwidth of linear and nonlinear Thomson scattering radiation for electron bunches with a finite energy spread. *Phys. Rev. Accel. Beams* **2021**, *24*, 020702. [CrossRef]
64. Bernhard, A.; Rodríguez, V.A.; Kuschel, S.; Leierb, M.; Peiffer, P.; Sävert, A.; Schwab, M.; Werner, W.; Widmann, C.; Will, A.; et al. Progress on experiments towards LWFA-driven transverse gradient undulator-based FELs. *Nucl. Instrum. Methods Phys. Res. Sect. A Accel., Spectrometers Detect. Assoc. Equip.* **2018**, *909*, 391–397. [CrossRef]
65. Qin, W.; Zeng, L.; Huang, S.; Zhao, G.; Ding, Y.; Huang, Z.; Hu, R.; Lu, H.; Yan, X.; Liu, K. Study of a free-electron laser driven by a laser-plasma accelerated beam at Peking University. *Nucl. Instrum. Methods Phys. Res. Sect. A Accel. Spectrometers Detect. Assoc. Equip.* **2019**, *925*, 193–198. [CrossRef]
66. Widmann, C.; Rodriguez, V.A.; Braun, N.; Nicolai, M.; Papash, A.; Reuter, M.; Rossmanith, R.; Sävert, A.; Werner, W.; Kaluza, M.C.; et al. Beam transport system from a laser wakefield accelerator to a transverse gradient undulator. In Proceedings of the 5th International Particle Accelerator Conference (IPAC 2014), Dresden, Germany, 15–20 June 2014; pp. 2803–2806.
67. Liu, T.; Huang, Z.; Liu, B.; Liu, J.S.; Wang, D.; Zhang, T. Beam Transport Line of the LPA-FEL Facility Based on Transverse Gradient Undulator. In Proceedings of the Seventh International Particle Accelerator Conference (IPAC 2016), Busan, Korea, 8–13 May 2016; pp. 3287–3290.

68. Jafarinia, F. Studies on Experiments and Free-Electron Laser Concepts with a Transverse Gradient Undulator. Ph.D. Thesis, Universität Hamburg, Hamburg, Germany. Available online: https://bib-pubdb1.desy.de/record/470631/files/Thesis.pdf (accessed on 20 November 2021).
69. Trebino, R. Optics Course, Lection 27. Available online: https://frog.gatech.edu/talks.html (accessed on 20 November 2021).
70. Ranjan, N.; Terzić, B.; Krafft, G.A.; Petrillo, V.; Drebot, I.; Serafini, L. Simulation of inverse Compton scattering and its implications on the scattered linewidth. *Phys. Rev. Accel. Beams* **2018**, *21*, 030701. [CrossRef]
71. Gu, X.; Akturk, S.; Trebino, R. Spatial chirp in ultrafast optics. *Opt. Commun.* **2004**, *242*, 599–604. [CrossRef]
72. Huang, Z.; Ding, Y.; Schroeder, C.B. Compact X-ray free-electron laser from a laser-plasma accelerator using a transverse-gradient undulator. *Phys. Rev. Lett.* **2012**, *109*, 204801–204805. [CrossRef] [PubMed]
73. Terzić, B.; Krafft, G.A.; Petrillo, V.; Drebot, I.; Ruijter, M. Improving inverse Compton sources by avoiding non-linearities. *EPL* **2020**, *129*, 62001. [CrossRef]